GEOPHYSICS, VOL. 78, NO. 5 (SEPTEMBER-OCTOBER 2013); P. H1–H11, 10 FIGS., 2 TABLES.
10.1190/GEO2012-0266.1

Effects of magnetite on high-frequency ground-penetrating radar

Remke L. Van Dam[1], Jan M. H. Hendrickx[2], Nigel J. Cassidy[3], Ryan E. North[4], Mine Dogan[1], and Brian Borchers[5]

ABSTRACT

Large concentrations of magnetite in sedimentary deposits and soils with igneous parent material have been reported to affect geophysical sensor performance. We have undertaken the first systematic experimental effort to understand the effects of magnetite for ground-penetrating radar (GPR) characterization of the shallow subsurface. Laboratory experiments were conducted to study how homogeneous magnetite-sand mixtures and magnetite concentrated in layers affect the propagation behavior (velocity, attenuation) of high-frequency GPR waves and the reflection characteristics of a buried target. Important observations were that magnetite had a strong effect on signal velocity and reflection, at magnitudes comparable to what has been observed in small-scale laboratory experiments that measured electromagnetic properties of magnetite-silica mixtures. Magnetite also altered signal attenuation and affected the reflection characteristics of buried targets. Our results indicated important implications for several fields, including land mine detection, Martian exploration, engineering, and moisture mapping using satellite remote sensing and radiometers.

INTRODUCTION

In recent years, there has been an increased interest in the effects of ferrimagnetic material on ground-penetrating radar (GPR) signal performance. This interest has been driven by the realization that soil mineralogy is of considerable importance for modern land mine detection sensors, which often use high-frequency GPR (Takahashi et al., 2011), by the plans to include a high-frequency GPR system on one of the future Mars rovers (e.g., Ciarletti et al., 2011), and by the increased use of high-frequency GPR systems in engineering fields where magnetic material is likely encountered (Cassidy and Millington, 2009). In addition, ferrimagnetic minerals in soils may affect retrieval of soil moisture using C- and L-band radiometers and microwave satellite sensors, although this is not discussed in the relevant literature (e.g., Jackson et al., 1999; Moran et al., 2004; Barrett et al., 2009). In all of the above cases, it is of critical importance that the potentially detrimental effects of ferrimagnetic material on system performance are considered and taken into account during the survey planning stages. However, to date, no controlled experiments have been conducted.

Iron oxides are common in many rock types and sedimentary deposits, as well as in soils in a wide range of different climates. Whereas the most ubiquitous iron oxides, goethite and hematite, have bulk electromagnetic properties similar to those of other common earth materials, ferrimagnetic minerals such as magnetite and maghemite exhibit different behavior. These minerals have a strong magnetic spin moment and can, even in small amounts, be detected in natural environments by their elevated magnetic susceptibility. This unique character has allowed study of the distribution of ferrimagnetic minerals in a wide range of fields, including among others, paleoclimatology (Maher and Thompson, 1995), soil development (Singer et al., 1996; Van Dam et al., 2008), and archeology (Benech and Marmet, 1999). In recent years, new interest in the issue of ferrimagnetic minerals in the environment has arisen due to the effect they can have on the performance of GPR and other electromagnetic sensors. Areas of particular interest are related to Mars exploration programs (Coey et al., 1990; Grant et al., 2003; Leuschen et al., 2003; Bertelsen et al., 2004; Stillman and Olhoeft, 2008; Ciarletti et al., 2011), the detection of unexploded ordnance (UXO) and land mines (Van Dam et al., 2005; Takahashi et al., 2011), and civil engineering applications such as imaging of

Manuscript received by the Editor 11 July 2012; revised manuscript received 1 April 2013   Published online 25 July 2013.
[1]Michigan State University, Department of Geological Sciences, East Lansing, Michigan, USA. E-mail: rvd@msu.edu; minedoga@msu.edu.
[2]New Mexico Institute of Mining and Technology, Department of Earth and Environmental Science, Socorro, New Mexico, USA. E-mail: hendrick@nmt.edu.
[3]Keele University, School of Physical and Geographical Sciences, Staffordshire, UK. E-mail: n.j.cassidy@esci.keele.ac.uk.
[4]United States Army Engineer Research and Development Center (ERDC), Vicksburg, Mississippi, USA. E-mail: ryan.e.north@usace.army.mil.
[5]New Mexico Institute of Mining and Technology, Department of Mathematics, Socorro, New Mexico, USA. E-mail: borchers@nmt.edu.

corroded steel-reinforced concrete and soils containing waste material of smelting operations (Cassidy and Millington, 2009).

It has long been known that magnetite and other ferrimagnetic minerals affect electromagnetic properties of soils and sediments (Robinson et al., 1994; Olhoeft, 1998; Klein and Santamarina, 2000). As has been shown in a few recent theoretical and laboratory studies, these altered electromagnetic properties may, in turn, lead to considerable changes in signal propagation at GPR-specific frequencies. For example, measurements of electromagnetic wave propagation through magnetite-silica mixtures using time-domain reflectometry (TDR) demonstrated that the presence of magnetite leads to a significant decrease in electromagnetic wave velocity (Mattei et al., 2005; Pettinelli et al., 2005). Recent measurements of electromagnetic properties for similar magnetite-silica mixtures using a vector network analyzer (VNA) showed a strong frequency-dependent effect of magnetite on propagation velocity and signal attenuation (Cassidy, 2008). This effect is stronger for nanoscale, single-domain, and low-order multiple-domain magnetite grains than for large, high-order multiple-domain grains. The results of these recent studies indicate that standard approaches for estimation of GPR signal behavior in soils and sediments, such as empirical relationships (e.g., Topp et al., 1980) and volumetric mixing models (e.g., the complex refractive index model), may not be reliable when even small amounts of ferrimagnetic minerals are present. Moreover, these results suggest that depending on how ferrimagnetic minerals are mixed, their presence can lead to signal reflection and scattering.

Although for many field conditions the concentration of ferrimagnetic minerals is considered too low to significantly impact GPR wave propagation, a few studies have reported signal reflections caused by magnetite concentrated in sediment layers. A study of near-shore marine deposits identified unusually strong reflections (bright spots) related to magnetite concentrations along the bedding planes of storm deposits (Jol et al., 1998; Peterson et al., 2010). In a study of the paleo markers in a relict eolian dune, strong reflections were related to the presence of heavy minerals, possibly magnetite (Buynevich et al., 2007). Despite the indication that anomalous magnetic properties of the layers of ferrimagnetic minerals may have caused these reflections, it is difficult to obtain conclusive evidence for these interpretations. Alternative explanations for the unusual reflection strengths associated with these heavy mineral concentrations are different textural properties such as porosity and bulk density (Neal, 2004), altered water retention characteristics (Van Dam and Schlager, 2000; Van Dam et al., 2002), and surface effects (Josh et al., 2011).

Despite new insights from laboratory studies into the effects of magnetite on electromagnetic wave propagation in soils and sediments, no practical GPR experiments to specifically study the effect of magnetite on GPR wave propagation and reflection have been made. Consequently, a thorough understanding of the potential effects of magnetite in the natural environment on GPR surveys is currently lacking. This study is the first direct analysis of the effects of magnetite on the performance of GPR systems. In a controlled laboratory setup, we measured the effects of magnetite on propagation velocity, signal attenuation, and reflection strength for different scenarios that represent two typical distributions of magnetite in natural environments. We compared our findings with results from previous laboratory experiments.

THEORETICAL BACKGROUND

The frequency-dependent properties that play a role in the behavior of the electromagnetic energy in a medium are the dielectric permittivity ε, the electrical conductivity σ, and the magnetic permeability μ. The complex dielectric permittivity is given by

$$\varepsilon_e^*(\omega) = \varepsilon_e'(\omega) + j\varepsilon_e''(\omega) = \varepsilon'(\omega) + j\left(\varepsilon''(\omega) + \frac{\sigma(\omega)}{\omega\varepsilon_0}\right), \tag{1}$$

where $\varepsilon_e^*(\omega)$ is the frequency-dependent, complex effective permittivity Fm^{-1}, $\varepsilon'(\omega)$ and $\varepsilon''(\omega)$ are the real and imaginary components of the frequency-dependent complex permittivity Fm^{-1}, respectively (effective permittivity using subscript e), and $\sigma(\omega)$ is the frequency-dependent electrical conductivity (Sm^{-1}). The electrical conductivity is often assumed noncomplex (Cassidy, 2009).

Similar to the complex permittivity, magnetically lossy materials have a complex magnetic permeability with a real and an imaginary part (Olhoeft and Strangway, 1974; Keller, 1987; Cassidy, 2008). This complex permeability is given by

$$\mu^*(\omega) = \mu'(\omega) + j\mu''(\omega), \tag{2}$$

where $\mu^*(\omega)$ is the frequency-dependent, complex magnetic permeability Hm^{-1} and $\mu'(\omega)$ and $\mu''(\omega)$ are the real and imaginary components of the frequency-dependent complex magnetic permeability Hm^{-1}.

Electrical conductivity describes the ability of an electric field to move free charges, such as electrons or ions, through a medium. The interaction of these moving charges with the medium results in energy losses. At low GPR frequencies, the movement of the charges is instantaneous, so that the conduction moves in phase with the electrical field. Under these conditions, the conductivity is given using a static (or DC) value, which is noncomplex. At high GPR frequencies, the response of the charges is noninstantaneous, which requires a complex description of the conductivity. It is nevertheless generally assumed that the imaginary component is small and can be ignored.

As electromagnetic energy moves through a medium, charges become displaced and polarized, resulting in a loss of energy. The frequency at which this polarization occurs is called the relaxation frequency. Relaxation mechanisms are frequency dependent and vary with material characteristics (Cassidy, 2009). A general description for the electromagnetic loss tangent is (Keller, 1987)

$$\tan\,\delta_{\mathrm{EM}} = \frac{\tan(\delta_M - \delta_E)}{2}, \tag{3}$$

in which the electric loss tangent is defined as $\tan\,\delta_E = (\sigma' - \omega\varepsilon'')/(\sigma'' + \omega\varepsilon')$ and the magnetic loss tangent is defined by the ratio of the imaginary and real components of the magnetic permeability $\tan\,\delta_M = \mu''/\mu'$. Here, σ' and σ'' are the real and imaginary components of the electrical conductivity Sm^{-1}.

Most permittivity relaxation mechanisms exhibit a gradual decrease of the real part of the permittivity with increasing frequencies and a peak of the imaginary part of the permittivity at the relaxation frequency. Permittivity relaxation mechanisms can be subdivided into free charge effects, which mostly occur at frequencies below

1 MHz, and molecular and atomic polarizations at typical GPR frequencies and above. For dry materials, such as in the experiments described in this paper, the most important loss mechanisms are electronic and atomic polarization, although these occur above the typical GPR frequency range (Cassidy, 2009). Another important dielectric loss mechanism, typically associated with interstitial fluids, is dipolar relaxation.

Similar to permittivity, the magnetic permeability of a material is frequency dependent. Low-frequency loss mechanisms are related to the movement of magnetic domain walls (Klein and Santamarina, 2000), the behavior of which depends on grain size and domain size, among other factors. At higher GPR frequencies, magnetic relaxation losses are small. In this frequency range, however, ferrimagnetic materials can have a distinct effect on the permittivity through conductive effects (Klein and Santamarina, 2000). These conductive effects vary with concentration of the ferromagnetic inclusions, their distribution, and shape. Thus, even as magnetic permeability and magnetic relaxation losses are small, ferrimagnetic inclusions can affect GPR wave velocity, amplitude, and phase (Klein and Santamarina, 2000).

The propagation velocity and signal attenuation of GPR waves depend on the above-defined electromagnetic properties and are thus frequency dependent. For a homogeneous, isotropic medium, the velocity and attenuation (in $\mathrm{dBm^{-1}}$) are given by (Daniels, 2004)

$$v(\omega) = c_0\left(\frac{\mu(\omega)\varepsilon'(\omega)(1+\sqrt{1+\tan^2\delta(\omega)})}{2\varepsilon_0\mu_0}\right)^{-0.5}, \quad (4)$$

$$\alpha(\omega) = 8.686\omega\left(\frac{\mu(\omega)\varepsilon'(\omega)(\sqrt{1+\tan^2\delta(\omega)}-1)}{2}\right)^{0.5}, \quad (5)$$

where c_0 is the velocity of electromagnetic waves in vacuum $\mathrm{ms^{-1}}$, $\tan\delta(\omega)$ is the frequency-dependent loss tangent of the material, ε_0 is the permittivity of vacuum $8.85419\times10^{-12}\ \mathrm{Fm^{-1}}$, and μ_0 is the magnetic permeability of vacuum $4\pi\times10^{-7}\ \mathrm{Hm^{-1}}$.

These equations for GPR signal velocity and attenuation incorporate lossy behavior or electrical properties through the loss factor, but they do not include possible loss mechanisms for magnetic properties. However, this is an acceptable simplification because the GPR data discussed in this paper were conducted at frequencies above the common magnetic relaxation frequencies.

EXPERIMENTAL PROCEDURE

Sample material

Experiments were performed using quartz-rich sand (QS) and natural crystalline magnetite. The QS was obtained from a site near the campus of New Mexico Tech in Socorro, New Mexico, and it consists of predominantly quartz mixed with plagioclase. The material was air dried for a week in the laboratory and then sieved through a 2-mm mesh, discarding all grains larger than sand size. The magnetite was obtained from the beach of Nueva Gorgona, Panama, 60 km southwest of Panama City, where it is found concentrated in thin layers or placer deposits (PDs) (Figure 1a). After two days of oven drying at around 45°C, the magnetite was magnetically separated from the regular beach sand in the samples; the beach sand was then discarded. The QS sample had a dry bulk density of $1.58\ \mathrm{g/cm^3}$; the magnetite sample had a dry bulk density of $2.48\ \mathrm{g/cm^3}$. The mean grain size of the QS is about double that of the magnetite (Figure 1b and 1c). The magnetite grains are quite well rounded, reflecting the depositional processes of a beach environment. A ZH Instruments SM-105 (513 kHz) was used to estimate the magnetic permeability for the magnetite sample. The estimated value (1.42) is lower than that for a laboratory-grade magnetite powder.

Electromagnetic properties

Measurement of the complex electromagnetic properties of the sample material was performed with a Hewlett-Packard (HP) Model 8753E VNA, controlled by a custom software program (Kutrubes, 1986; Olhoeft and Capron, 1993; Canan, 1999). The 16 independent measurements were performed over a frequency range of 30 kHz to 3 GHz at 401 discrete log-spaced frequencies and averaged. At low frequencies, the quality of the data is impacted by diffusive field behavior (Annan, 2009). At high frequencies, the data are affected by sample holder resonance. The frequency range over which the data were physically representative was 0.1–1.8 GHz. The samples were loaded into a 3-cm-long General Radio GR900 air line with Teflon ends caps. Each sample holder was weighed empty and full to allow calculation of the sample bulk density. The VNA was calibrated with a full two-port short/open/load/through procedure: first for the cables alone with an HP calibration kit, then including the APC-7 7 mm to GR900 adapter with a General Radio GR900 calibration kit. A test measurement of air was performed prior to measurement of the soil samples to verify correct system response. The S-parameters were plotted during collection to ensure that the forward and reverse parameters agreed. The four S-parameters (S11, S12, S21, S22) were calculated using

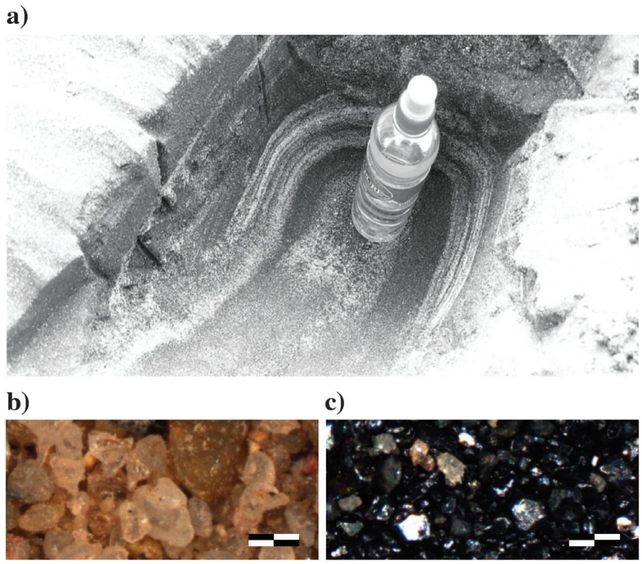

Figure 1. (a) Magnetite used in this study was obtained from the beach of Nueva Gorgona, Panama, where it is found concentrated in thin layers. (b) Close-up photograph of quartz sand from New Mexico. (c) Close-up photograph of magnetite from Panama. The length of the scale bar in (b, c) is 500 μm.

the Nicolson-Ross-Weir algorithm to determine the complex dielectric permittivity, magnetic permeability, electrical loss tangent, magnetic loss tangent, and electrical resistivity. For comparison, additional measurements were performed using an Agilent 85070E high-temperature probe and an Agilent FieldFox N9912A VNA over the frequency range of 10 MHz to 4 GHz. These alternative lab setups produced similar results.

Ground-penetrating radar experiments

GPR experiments were performed in a wooden test box with internal dimensions of $0.5 \times 0.31 \times 0.29$ m ($l \times w \times h$). The box, with a wall thickness of 0.01 m, stood on a wooden desk 0.02-m thick,

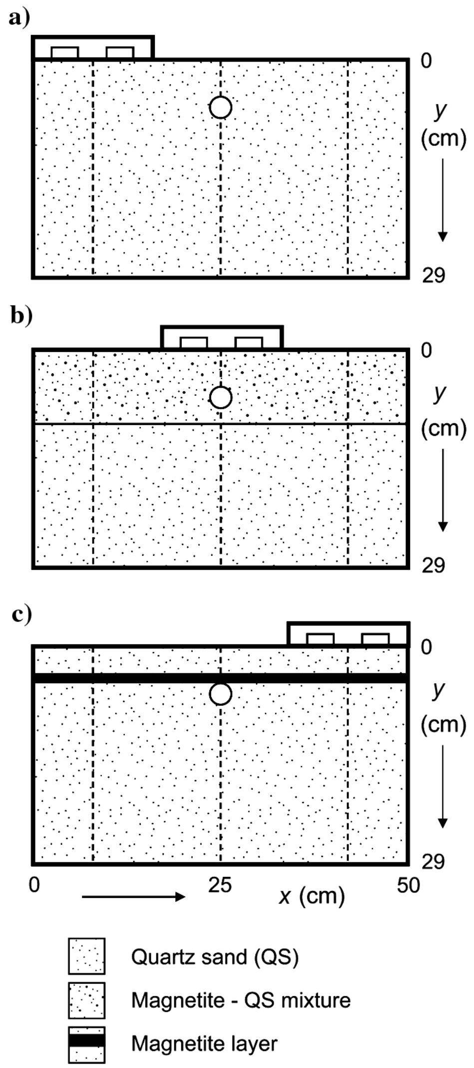

Figure 2. Experimental design for different scenarios. The scenarios include (a) background measurements in QS, (b) 0.1-m-thick homogeneous mixtures of magnetite and QS (9.1% and 22% magnetite by weight) above QS, and (c) a 0.015-m-thick layer (PD) of pure magnetite interbedded between two QS units. The dashed vertical lines represent the locations of the first and last measurement at 0.08 and 0.42 m, respectively, and the central point ($x = 0.25$ m). The open circle at 0.05 m below the surface represents the steel ball with one-inch (0.026-m) diameter used as target in some of the measurements.

above air. The GPR equipment used was a Sensors & Software pulseEKKO 1000 system with shielded 1.2-GHz antennas in a bistatic coplanar configuration. For measurements in background material and in homogeneous mixtures of QS and magnetite, the signal had a broad-peaked frequency spectrum centered at around 1.08 GHz and a plateau between 0.95 and 1.21 GHz. For measurements with shallow reflectors (layer of pure magnetite or buried target), the frequency spectrum broadened further, with a plateau between around 0.75 and 1.5 GHz. The peak frequency increased to 1.25 GHz. This change relative to the background frequency spectrum is likely not the result of different material electromagnetic properties or coupling effects, but rather due to interference between the reflected signal and the direct waves (Di Matteo et al., 2013).

Data were collected along the centerline of the test box, using a step size of 0.01 m; the antennas were placed directly on the surface. In all runs, the time window was 15 ns, with a sampling rate of 0.05 ns (300 samples per trace). To ensure high data quality, 128 stacks were averaged to form each trace. With start and end positions of 0.08 and 0.42 m, respectively, each transect consisted of 35 traces. All runs were conducted using bistatic copole configuration transverse and parallel to the survey line. The difference in signal characteristics was negligible, except in the presence of the buried target. Unless otherwise specified, the data presented in this paper were collected using a transverse antenna orientation.

Results of the experiments are presented as either A-scans in the center of the box ($x, y = 0.25, 0.155$ m), or as B-scans. The A-scans present a single trace (128 stacks) of signal amplitude versus two-way traveltime. A-scans have been corrected for time-zero shifts and normalized to the maximum absolute amplitude observed in all A-scans. As the traces were very clear, no further processing has been applied. The B-scans are 2D cross sections (variable density plots of signal amplitude) showing two-way traveltime versus distance. B-scans have been processed using a dewow filter and a DC shift application to compensate for long-term instrument drift. To enhance the visibility of lower amplitude reflections off a buried target and the bottom of the test box, the B-scans have been processed with a function for automatic gain control (AGC).

Experimental scenarios

Different scenarios were used to understand the effect of magnetite on GPR signals (Figure 2). The scenarios were designed to be representative of two common types of occurrence of magnetite in natural environments. The first type is homogeneous mixtures of magnetite and QS (Figure 2b). In natural environments, after the magnetite is separated through physical or chemical weathering of magnetite-rich rocks, homogeneous mixtures can develop by redistribution in soils or by reworking through sedimentary agents. The second type is a thin layer of magnetite sandwiched between QS (Figure 2c). In field settings, the contrasting grain density of magnetite and quartz sand can lead to selective transport and deposition. These types of deposits are referred to as PDs and are commonly found where high-density minerals are concentrated in eolian, fluvial, marine, and coastal sediments (Figure 1a) by waves or current action (Komar and Wang, 1984). In addition, background measurements on magnetite-free QS material were performed to test the experimental setup and improve data reduction (Figure 2a).

The mixture scenario was designed to primarily study the effect of magnetite on signal velocity and dispersion. Mixtures of QS and magnetite were prepared in two different weight proportions (9.1% and 22% magnetite by weight). First, the lower part of the box was filled with QS. The upper 0.1 m of the box was then filled with magnetite-sand mixtures (Figure 2b). The magnetite-sand mixture was limited to the upper part due to the total available quantity of magnetite (~500 g) and to allow the use of significant concentrations of magnetite. The magnetite-sand mixture was separated from the QS below using a thin paper divider that did not impact GPR signals.

The layer scenario, with a layer of pure magnetite resembling a PD, was primarily designed to study the effect of magnetite on GPR signal reflection characteristics, although observations on signal velocity are also made. The 0.015-m-thick layer was sandwiched between QS. The top of the layer was at 0.035 m below the surface (Figure 2c). Separation of materials was achieved by thin paper dividers that did not have an impact on the GPR signals. The amount of magnetite used for this experiment was the same as what was used for the homogeneous mixture with 22% magnetite by weight.

To further study the effect of the presence of magnetite on reflection characteristics, a stainless steel ball of 1-in diameter was used as a target for each of the scenarios (QS background, homogeneous mixtures of QS and magnetite, and a PD). The target was buried within the QS and homogeneous magnetite-sand mixtures, and below the magnetite PD, with its top at 0.05 m below the sediment surface (Figure 2).

RESULTS

Electromagnetic properties

The complex dielectric permittivities of the QS and magnetite samples are shown in Figure 3. The relative permittivity of QS is around 2.8 and, as expected, exhibits no frequency dependence (Figure 3a); the imaginary component is near zero (Figure 3b). The relative permittivity of the magnetite is much higher and shows strong frequency dependence in real and imaginary components. A similar increase at low frequencies is observed by Cassidy (2008) and Pettinelli et al. (2005). At the center frequency of the GPR signal (1.08 GHz), the relative permittivity of the magnetite is around 8.4 (Figure 3a). The measured complex behavior of the sample material is comparable to earlier measurements on quartz and magnetite powders (e.g., Cassidy, 2008), although there is no exact match. The differences may be due to the sample characteristics and measurement methodology.

The complex magnetic permeability of both samples differs only slightly (Figure 4) and exhibits no significant frequency dependence. The absence of a relaxation peak at megahertz frequencies (e.g., Olhoeft and Strangway, 1974; Stillman and Olhoeft, 2008) may be due to the diffusive field behavior at these frequencies (Annan, 2009). The relative magnetic permeability of QS is, as expected, around one. The relative magnetic permeability of magnetite is only slightly higher (Figure 4a). This observation is supported by independent measurements of magnetic susceptibility using a ZH Instruments SM-105. The imaginary components of both samples are very small. As most magnetic relaxation losses occur below 0.1 GHz (e.g., Cassidy, 2009), the increase in the imaginary component of the magnetite sample between 0.5 and 1.5 GHz (Figure 4b) is most likely an artifact of the measurement procedure.

The electrical conductivity response for both sample materials is significantly larger for magnetite than for quartz sand (Figure 5a), as

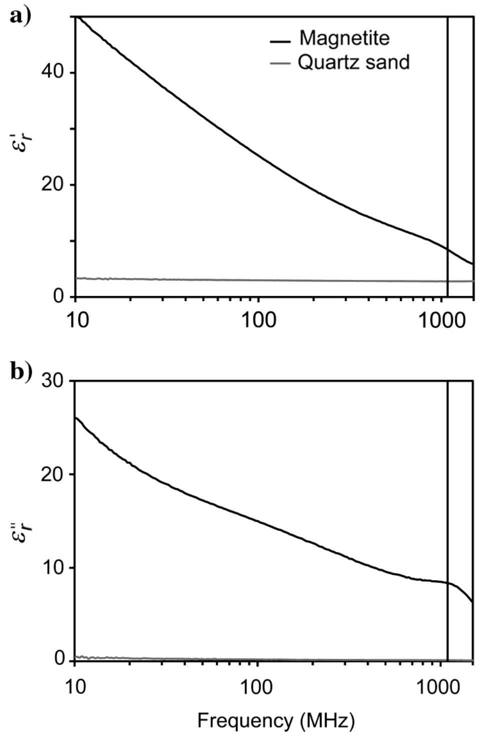

Figure 3. Plots of complex dielectric properties of the sample material: (a) real part of the dielectric permittivity and (b) imaginary part of the dielectric permittivity. The center frequency of the GPR signal for scenarios with QS and QS + M mixtures (1.08 GHz) has been indicated using a solid vertical line.

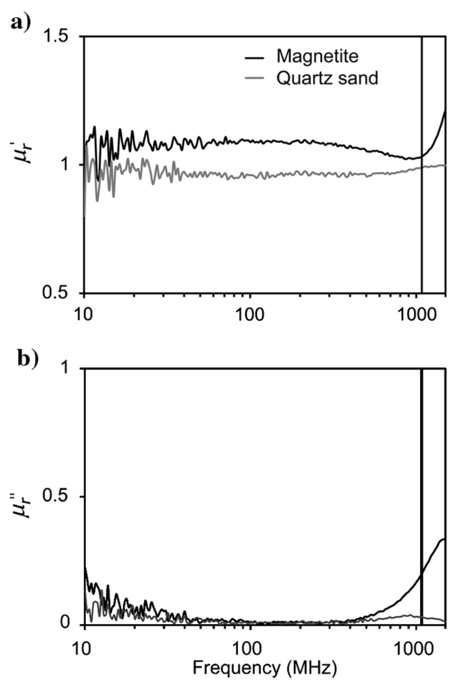

Figure 4. Plots of complex magnetic permeability of the sample material: (a) real part of the magnetic permeability and (b) imaginary part of the magnetic permeability. The vertical solid line indicates the center frequency of the GPR signal.

is also evident from the calculated electrical loss tangent (Figure 5b). The conductivity increases with frequency and reaches around 0.5 Sm^{-1} at the GPR center frequency. The conductivity is expected to have a significant effect on signal velocity, attenuation, and dispersion. The rapid increase in the magnetic loss tangent at frequencies near the center frequency of the GPR signal (Figure 5c) is an artifact of sample holder resonance and is related to the same feature in Figure 4b.

Ground-penetrating radar results

The dry wood of the sample box and the table has dielectric properties close to that of dry sand (Grosvenor et al., 2009). It is therefore expected that the wood-to-air transition at a depth of 0.32 m (0.29 m sample material + 0.03 m wood) will produce the most prominent reflection of GPR energy. This reflection will be used to assess changes in velocity and attenuation due to the presence of magnetite in the mixture and layer scenarios. Arrival times of the direct waves and the reflection from the bottom of the box were determined using a Hilbert transform as an envelope detection tool.

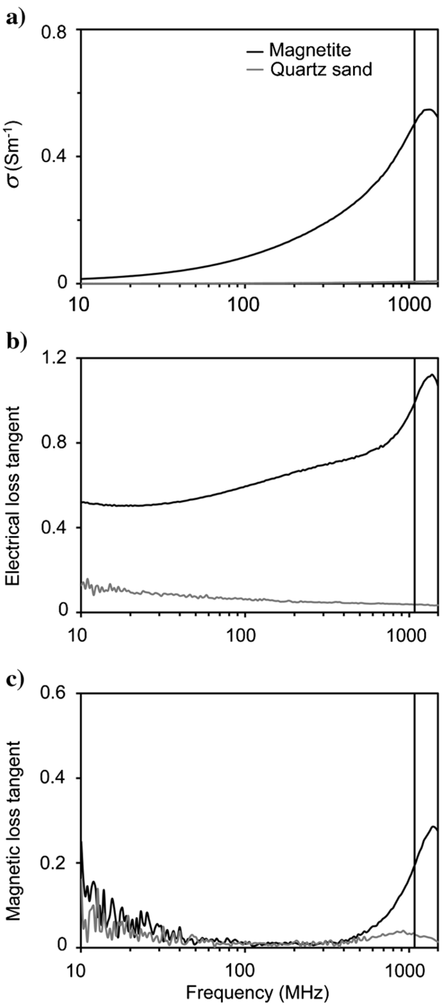

Figure 5. Plots of (a) electrical conductivity, (b) electrical loss tangents, and (c) magnetic loss tangents for the sample material. The vertical solid line indicates the center frequency of the GPR signal.

Homogeneous sand (QS)

GPR data for the QS-filled test box without added magnetite or targets displays a strong signal from the direct air and ground waves between approximately 0 and 2 ns (Figure 6). The reflection from the bottom of the box (wood-to-air transition) is seen at around 4.2 ns two-way traveltime (Table 1). This traveltime can be translated into GPR signal velocity using $v = 2d/t$, where d is the height of the test box (0.29 m) plus the thickness of the wood.

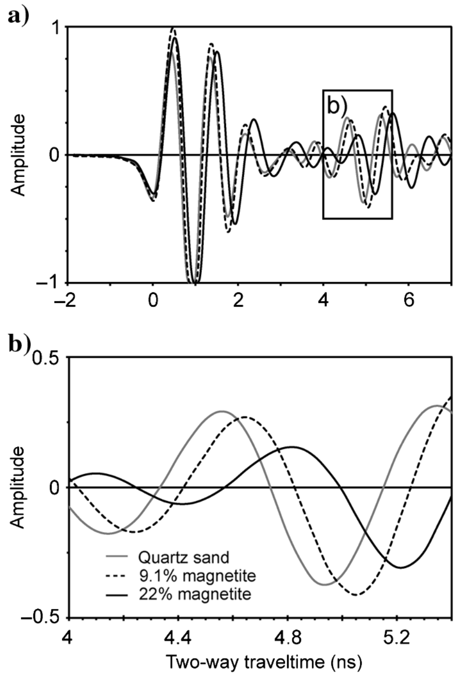

Figure 6. (a) GPR A-scans of QS background reading and magnetite-sand mixtures of varying concentration. (b) Close-up of the bottom reflection for the three measurements.

Table 1. Velocity calculations for GPR measurement scenarios of QS, homogeneous mixtures of QS and magnetite (at 9.1% and 22% weight of magnetite), and 100% magnetite in a PD.

	QS	QS + M (9.1%)	QS + M (22%)	PD
Material order	QS	QS + M, QS	QS + M, QS	QS, M, QS
Layer boundaries (m)	—	0.1	0.1	0.035, 0.05
$\mathrm{TWT}_{(T)}$ (ns)	4.2	4.3	4.55	4.4
$d_{(\mathrm{QS})}$ (m)	0.32	0.22	0.22	0.305
$d_{(M)}$ (m)	0	0.1	0.1	0.015
$v_{(T)}$ (m/ns)	0.152	0.149	0.141	0.145
$v_{(M)}$ (m/ns)	—	0.142	0.120	0.076

The subscript T denotes total thickness, which includes all sediment layers and wood below the material. The subscript M indicates magnetite or QS-magnetite mixture. The estimated velocity for QS (0.152 m/ns) and the known thickness of the layers containing magnetite ($d_{(M)}$) are used to calculate $v_{(M)}$.

The electromagnetic wave velocity is therefore equal to $0.64/4.2 = 0.152$ m/ns, which is a typical value for dry sand. The velocity would increase by less than 1% when incorporating the antenna separation in this calculation. In the zone between the direct arrivals and the bottom reflection, the data are largely free of noise. The amplitude of horizontal events in the data (direct waves and bottom reflection) can be suppressed by subtracting the 35-trace average from each individual trace in the 2D data set. This reveals the presence of some reflections that dip downward toward the center of the survey line. These dipping reflections originate from the bottom edges of the box. However because these reflections are of very low amplitude and start after 5 ns, they do not impact our analysis of the bottom reflection significantly.

Homogeneous magnetite-sand mixtures

GPR A-scans for homogeneous magnetite-sand mixtures are shown in Figure 6 and compared with the background QS measurement. The most prominent effect of the presence of magnetite is the delayed arrival time of the reflection from the bottom of the box (Figure 6b). The arrival time for the box-to-air transition has increased from 4.2 ns for the QS experiment to 4.3 and 4.55 ns for the 9.1% and 22% magnetite experiments, respectively. This increase, due to the presence of the magnetite-sand mixture in the upper part of the box, corresponds to a significant reduction in velocity. Using the known thickness of the magnetite-sand mixture (0.1 m) and the known velocity for the QS below (0.152 m/s), the velocity change can be calculated. For the mixture with 9.1% magnetite, the GPR signal velocity is 0.142 m/ns. For the mixture with 22% magnetite, the signal velocity is 0.120 m/ns. Compared to the velocity in QS, this amounts to velocity decreases of 7.1% and 21.1%, respectively.

Other changes in the GPR signal that were observed during experiments with magnetite-sand mixtures are as follows: (1) apparent signal dispersion of the direct wave arrival (widening of the pulse) at the highest concentration and (2) a lower amplitude of the reflection of the bottom of the box.

The pulse widening of the first arrivals (Figure 6a) is likely the result of changes in the convoluted signal of the direct air and ground waves (e.g., Di Matteo et al., 2013). In this case, these changes are due to the lower GPR wave velocity in the magnetite-sand mixture, which causes a slightly delayed (but not decoupled) arrival of the direct ground wave. The pulse widening may also be a result of antenna-ground coupling effects that are different for each scenario (Annan, 2009). The observed pulse widening may also be a true dispersion effect, caused by the high electrical conductivity of the magnetite (Figure 5a). However, no pulse widening is seen for the reflection from the bottom of the box (Figure 6b), which suggests that the amount of dispersion is small at these concentrations of magnetite.

The lower signal amplitude that is observed for the bottom-of-the-box reflection (Figure 6a), is most pronounced for the mixture with 22% magnetite. Only a minor amplitude reduction is seen for the mixture with 9.1% magnetite. The lower signal amplitude is caused by increased signal attenuation in the magnetite-sand mixture and the partial reflection of the GPR signal at the boundary between the magnetite-sand mixture and QS below at 0.1 m depth has lowered the amount of propagating energy.

In the next two sections, the results are described for signal behavior in the presence of a 0.015-m-thick layer of pure magnetite, designed to resemble a PD, and for measurements over a 1-inch diameter steel target (M1) buried in the measurement box. The magnetite layer and the buried steel ball are located at a depth where their responses interfere with the direct air and ground waves. This shallow depth was chosen so that the results are relevant for real-world scenarios with shallow targets, such as buried land mines and UXO.

Magnetite layer (PD)

The GPR measurement for the magnetite layer is presented in comparison with the response for QS (Figure 7). This comparison shows that the addition of the magnetite results in significant changes to the signal response. The most prominent effect of the presence of the magnetite layer is the large change in the signature of the direct wave arrivals between around 0.8 and 2.0 ns. This change is likely a direct result of the signal reflection from the boundary between QS and the magnetite at a depth of 0.035 m. In addition, the signal characteristics are likely altered by the different propagation of the ground wave. The presence of the lower-velocity magnetite layer turns the overlying QS layer into a thin high-velocity waveguide (e.g., Liu and Arcone, 2003; Strobbia and Cassiani, 2007; van der Kruk et al., 2009).

Other changes in the GPR signal that were observed during the experiments with the magnetite layer are (1) a delayed arrival time of the reflection from the bottom of the box and (2) a lower amplitude of the reflection from the bottom of the box. Both effects were also observed for the scenario with homogeneous magnetite-sand mixtures.

The reflection from the bottom of the box exhibits a time delay of around 0.2 ns (Figure 7, Table 1), although this estimate is likely affected by the near-field effects of the PD layer on the shape of the direct waves and reflection. As before, in the experiments with homogeneous magnetite-sand mixtures, the increase in traveltime corresponds to a significant reduction in velocity. Using the thickness of the layer (0.015 m) and the known velocity for the QS (0.152 m/s), the GPR signal velocity through the magnetite is calculated as 0.076 m/ns. Compared to the velocity in QS, this is a velocity decrease of 50.4%.

The lower signal amplitude for the reflection of the bottom of the box (Figure 7) is similar in magnitude to the homogeneous mixture with 22% magnetite (Figure 6). The lower amplitude is caused by signal attenuation within the magnetite, in combination with

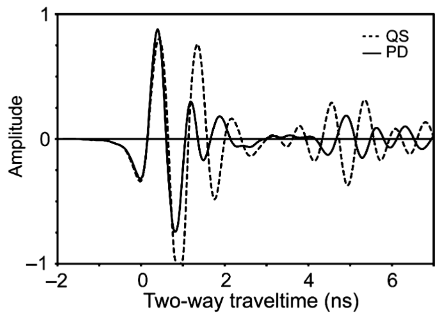

Figure 7. GPR A-scan of the 0.015-m-thick layer of magnetite bordered by QS above and below. A-scan of QS background measurement (same as in Figure 6) is shown for comparison.

reflection losses at the upper and lower boundaries of the magnetite layer. An additional modeling effort would be needed to explain these changes quantitatively.

Reflection target (M1)

Further evidence that magnetite has a strong effect on GPR signal behavior comes from experiments conducted with the steel target, buried in the test box. Compared with the background reading for no-target, no-magnetite QS, the steel target results in a clear deviation at early times (~1–3 ns), as would be expected due to the large dielectric contrast between the sand and steel (Figure 8, black and blue lines). The hyperbolic reflection associated with the target is well developed, but due to destructive interference with the direct waves, its amplitude is strongly reduced at the apex (Figure 9a), as is also observed in the A-scan (Figure 8, blue line). Compared with the background reading (Figure 8, black line), the presence of the target does not significantly alter the reflection from the bottom of the box. This is likely due to the relatively small size of the target (0.026 m) compared with the antenna separation (0.075 m) and signal wavelength (~0.13 m).

It is worth noting that interference patterns will differ with antenna frequency and orientation, material properties, and target contrast and burial depth. Indeed, the addition of magnetite changes the reflection signatures associated with the steel target. For the scenario with the ball buried at the same depth directly beneath the 0.015-m-thick magnetite layer, the GPR signal at early times is close to its background shape (Figure 8, red line), which is the combined result of all near-field effects. The signal amplitude of the hyperbolic response that is associated with the target has been significantly reduced, also where there is no interference with the direct waves (Figure 9b). This observation is a strong indication that the magnetite causes signal attenuation. In addition, the magnetite layer may act as a low-velocity waveguide (van der Kruk et al., 2009), leading to signal loss.

For the experiments with the magnetite layer and the magnetite-sand mixture (Figure 8, red and green lines), the reflection from the bottom of the box is strongly delayed, compared with the measurements without magnetite, with or without the target (Figure 8, black and blue lines). Hilbert transforms of the traces confirm these arrival

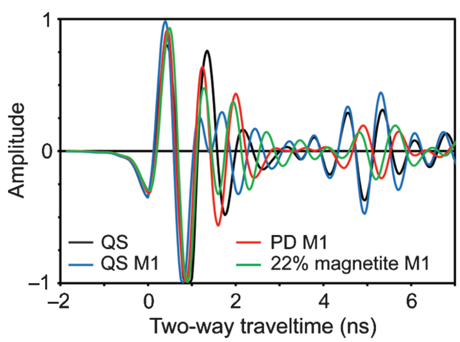

Figure 8. GPR A-scans of a one-inch steel target buried in QS (blue), below the 0.015-m-thick layer of pure magnetite (red), and in a magnetite-sand mixture (green). The background measurement for the no-target, no-magnetite experiment (QS) is shown in black.

time increases. This again demonstrates the impact of the presence of magnetite on the propagation velocity of GPR signals.

DISCUSSION

Our experimental results indicate that the presence of magnetite in soil material or sediment has a significant effect on the behavior of high-frequency GPR waves. In this section, we discuss our results in the context of variables most relevant to GPR sensor performance, which are signal velocity (which in turn governs signal reflection) and attenuation, and compare our results with previous theoretical and laboratory research.

Signal velocity

The electromagnetic wave velocity was estimated from GPR traveltime measurements in QS, homogeneous mixtures with 9.1% and 22% magnetite by weight, and for 100% pure magnetite. The velocity for these four experiments varied between 0.152 m/ns for the QS and 0.076 m/ns for pure magnetite (Figure 10). Although the total number of measurements is small, the consistent decrease in velocity with increasing magnetite concentration gives confidence that this relationship is valid and repeatable. Indeed, the measurements for comparable scenarios (QS, PD, mixtures) but with the buried steel target produced similar effects with respect

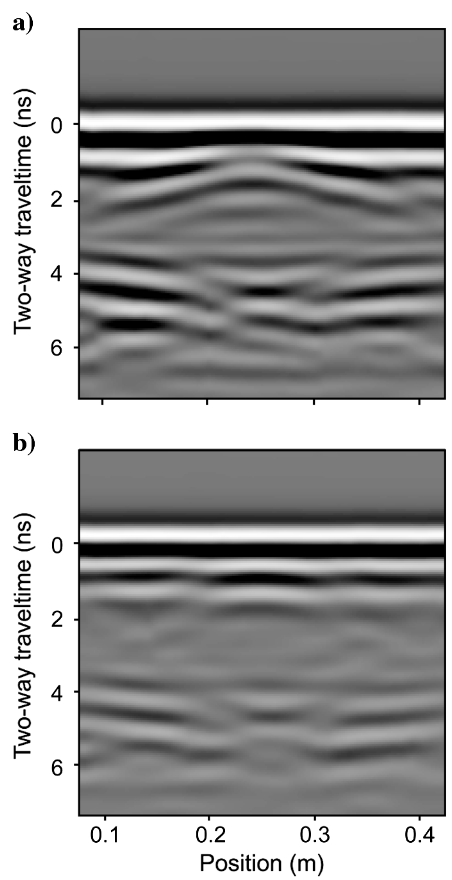

Figure 9. B-scans of the one-inch steel ball buried in (a) QS and (b) below the 0.015-m-thick layer of pure magnetite. Data were processed using signal dewow, DC shift, and AGC gain.

to the arrival time delay (and thus velocity retardation) of the reflection from the bottom of the box (Figure 8). The velocity results were compared with two recent studies from literature that measured electromagnetic wave properties using a VNA and TDR.

Measurements of the frequency-dependent velocity and attenuation characteristics for magnetite-silica mixtures were recently reported by Cassidy (2008). These measurements were performed using a VNA over the frequency range of 0.02–30 GHz for a series of powdered mixtures with a volume percent range of 0%, 1.5%, 2.6%, 5.4%, 8.2%, 11.3%, 17.9%, 25.3%, 33.7%, 43.3%, 60.4%, and 100% magnetite (0%, 3%, 5%, 10%, 15%, 20%, 30%, 40%, 50%, 60%, 75%, and 100% magnetite when converted to weight percent). The magnetite used was a commercially available kind at nano-to-micro grain sizes. Pettinelli et al. (2005) performed measurements of the electromagnetic wave velocity of magnetite-silica mixtures with a volume percent range of 0%, 5%, 10%, 15%, 20%, and 25% magnetite (0%, 9%, 17%, 25%, 32%, and 39% magnetite when converted to weight percent). The magnetite had grain sizes ranging from 200 to 500 μm, and was extracted from a beach (similar to the sample material used in this study). These measurements were performed using a TDR system and inverted to obtain responses over a broad frequency range from 0.01 to 0.5 GHz. This range encompasses the zone above 0.1 GHz, where velocity is nearly independent of frequency, as well as that below 0.1 GHz, where velocity drops with frequency (Cassidy, 2008).

The results of the velocity comparison are shown in Figure 10. In all studies, the background material is slightly different, but it is dominated by silica, and it is free of magnetite. All three studies show a significant decrease in velocity with increasing amount of magnetite (Figure 10a). The data by Pettinelli et al. (2005) and Cassidy (2008) are nearly identical. The data by Cassidy, which like the present study cover the full range of distributions from 0% to 100% magnetite, display a slight nonlinear response. For the end member case of 0% magnetite, the GPR velocity reported in this study matches the electromagnetic wave velocities from both earlier laboratory studies very well (Figure 10a). For the case with 100% magnetite, however, the GPR velocity is slightly higher than for the data from Cassidy (2008). This weaker match is possibly related to the near-field effects in the PD scenario on arrival time picks, as discussed previously. When focusing on velocity retardation, normalizing the velocity difference for the velocity in the background material, the results between the three studies show a very strong similarity (Figure 10b).

Based on the measured velocities for the different concentrations of magnetite, the expected reflection coefficients were calculated using $R = (V_1 - V_2)/(V_1 + V_2)$. Results are given in Table 2. Reflection coefficients for a normally incident wave at a planar boundary between QS ($v = 0.152$ m/ns) and layers with 9.1%, 22%, and 100% magnetite are 0.037, 0.118, and 0.337, respectively. Velocities calculated from the VNA measurements (Figures 3–5 and equation 4) are somewhat higher, but the calculated reflection coefficient between magnetite and QS is comparable at 0.290 (Table 2). These results show that even small quantities of magnetite can produce reflections similar to what is typical for sedimentary environments ($R \sim 0.05$ to 0.1). At higher concentrations of magnetite, bright spots can develop, similar to strong reflectors in sedimentary settings (reflection coefficients between around 0.2 and 0.4 for unsaturated sand to silt and groundwater table in coarse sand, respectively).

Signal attenuation

Increased signal attenuation for magnetite is reported by Pettinelli et al. (2005) and Cassidy (2008). As shown by both, attenuation is strongly frequency dependent, with significantly higher attenuation for increased frequency and magnetite concentration. Cassidy (2008) also demonstrates that this relationship is dependent on grain size. Between nano-to-micro grain size magnetite and a

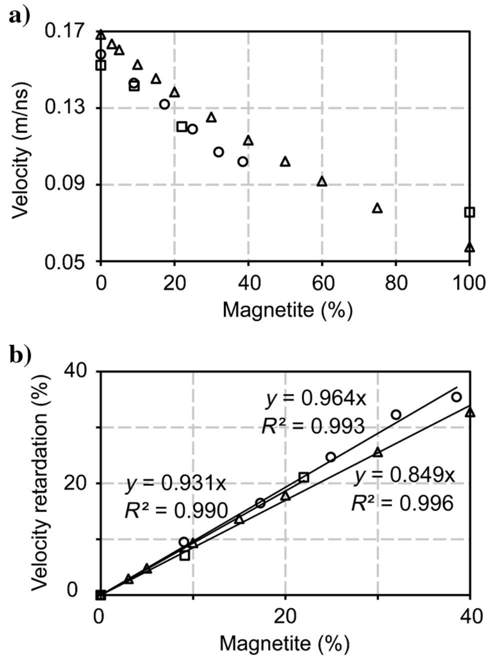

Figure 10. Comparison of velocity characteristics between this study (square symbols) and those from previous laboratory studies (Pettinelli et al., 2005, circles; Cassidy, 2008, triangles). All magnetite concentrations are in weight percent. (a) Velocity versus magnetite concentration. (b) Retardation in GPR signal velocity as a function of the magnetite concentration, relative to the velocity in QS for magnetite concentrations below 40%.

Table 2. Calculations of GPR wave velocity and reflection coefficients for QS, homogeneous mixtures of QS and magnetite (at 9.1% and 22% weight of magnetite), and 100% magnetite in a PD.

	Ground-penetrating radar		Vector network analyzer	
	v (m/ns)	R (with QS)	v (m/ns)	R (with QS)
0% magnetite (QS)	0.152	—	0.180	—
9.1% magnetite	0.142	0.037	—	—
22% magnetite	0.120	0.118	—	—
100% magnetite	0.076	0.337	0.099	0.290

Equation 4 was used to calculate the velocity for VNA measurements.

natural crystalline magnetite with larger predominant grain sizes of 0.1–3 mm, the natural crystalline magnetite displayed distinctly less frequency-dependent behavior (Cassidy, 2008). Also, the loss tangent, and thus attenuation, was significantly reduced for the natural magnetite. The real part of the dielectric permittivity, and thus velocity and reflection coefficients, was only marginally smaller.

The data collected in the present study are not ideally suited to quantify attenuation. It can be assumed, however, that for all scenarios tested (the measurements with the reflection target not included), the spreading and scattering losses are approximately equal. Thus, after correction for reflection losses, it may be possible to assess differences in signal attenuation using the reflection from the bottom of the box. In future work, these ideas can be tested via the modeling of reflective and dispersive GPR signal behavior for these scenarios.

CONCLUSIONS

This paper reports on the first set of laboratory experiments to assess the effects of magnetite in natural environments on GPR signal performance. Different realistic scenarios for the occurrence of magnetite in soils and sediments were considered and compared with background measurements on magnetite-free QS. In these scenarios, high-frequency GPR data were collected over homogeneous mixtures of QS and magnetite and for a layer of 100% magnetite, designed to resemble a so-called PD. Finally, all scenarios (including the background measurements) were repeated using a steel ball of one-inch diameter at shallow depth, to assess the effects of magnetite on the reflection characteristics of a buried target.

The results from this experimental study on dry material show that the presence of magnetite leads to a significant reduction in propagation velocity of GPR waves. Measurements on samples with only QS, and for homogeneous mixtures with 9.1% and 22% magnetite by weight, respectively, show a linear relationship between velocity and magnetite concentration. The velocity for 100% magnetite is close to that of typical values for saturated sand. The results obtained in this study largely confirm earlier laboratory measurements (using TDR and a VNA) on similar mixtures of magnetite and silica material from which the GPR signal velocity was deduced.

The change in wave velocity with magnetite concentration has a distinct effect on the reflection of GPR energy at layer boundaries. The results show that for even small amounts of magnetite, the reflection characteristics are similar to that of typical sedimentary layer boundaries. Moderate concentrations of magnetite may lead to bright spots (high amplitude reflections) in data, and magnetite placers (close to 100% concentration) can cause reflection strengths comparable to that of the largest contrast in sedimentary environments, which is the groundwater table boundary.

Magnetite had a significant effect on GPR signal attenuation. Measurements over a thin layer of 100% magnetite showed that the reflection strength of a steel target buried below the layer was significantly reduced. This was a direct result of attenuation within the magnetite. Other measurements, including reflections from the bottom of the test box also suggested that magnetite increased attenuation. Future modeling of this system, including the signal dispersion and reflections at layer boundaries, is needed to quantify the attenuation.

The results presented in this paper highlight the importance of magnetic properties on GPR signal performance, a variable that is routinely neglected or ignored. From these studies, it is also possible to identify a few avenues for future research. First of all, a better assessment needs to be made as to the effect of magnetite on GPR signal attenuation. For this purpose, a different experimental setup may need to be designed. Also, as has been shown by earlier laboratory studies, the relationship between magnetite concentration and GPR signal characteristics, in particular the attenuation, is strongly frequency dependent. It would therefore be desirable to conduct controlled GPR measurements over a range of antenna frequencies. Finally, measurements should be conducted in natural field settings, to assess the effects of heterogeneous distributions of magnetite on reflection, scattering, and attenuation.

ACKNOWLEDGMENTS

RVD and BB were funded for this research by the United States Army Research Office (STIR19-02-1-027). JH acknowledges support from the United States Army Yuma Proving Ground for sample collection in Panama. RN was granted permission to publish by the director of the Geotechnical & Structures Laboratory. We thank three anonymous reviewers and the associate editor for their suggestions to improve the manuscript.

REFERENCES

Annan, A. P., 2009, Electromagnetic principles of ground penetrating radar, *in* H. M. Jol, ed., Ground penetrating radar: Theory and applications: Elsevier, 3–40.

Barrett, B. W., E. Dwyer, and P. Whelan, 2009, Soil moisture retrieval from active spaceborne microwave observations: An evaluation of current techniques: Remote Sensing, **1**, 210–242, doi: 10.3390/rs1030210.

Benech, C., and E. Marmet, 1999, Optimum depth of investigation and conductivity response rejection of the different electromagnetic devices measuring apparent magnetic susceptibility: Archaeological Prospection, **6**, 31–45, doi: 10.1002/(SICI)1099-0763(199903)6:1<31::AID-ARP112>3.0.CO;2-N.

Bertelsen, P., W. Goetz, M. B. Madsen, K. M. Kinch, S. F. Hviid, J. M. Knudsen, H. P. Gunnlaugsson, J. Merrison, P. Nørnberg, S. W. Squyres, J. F. Bell, K. E. Herkenhoff, S. Gorevan, A. S. Yen, T. Myrick, G. Klingelhöfer, R. Rieder, and R. Gellert, 2004, Magnetic properties experiments on the Mars Exploration Rover Spirit at Gusev Crater: Science, **305**, 827–829, doi: 10.1126/science.1100112.

Buynevich, I. V., A. Bitinas, and D. Pupienis, 2007, Lithological anomalies in a relict coastal dune: Geophysical and paleoenvironmental markers: Geophysical Research Letters, **34**, L09707, doi: 10.1029/2007GL029767.

Canan, B., 1999, Dielectric properties of clay-water-organic compounds: Ph.D. thesis, Colorado School of Mines.

Cassidy, N. J., 2008, Frequency-dependent attenuation and velocity characteristics of nano-to-micro scale, lossy, magnetite-rich materials: Near Surface Geophysics, **6**, 341–354, doi: 10.3997/1873-0604.2008023.

Cassidy, N. J., 2009, Electrical and magnetic properties of rocks, soils and fluids, *in* H. M. Jol, ed., Ground penetrating radar: Theory and applications: Elsevier, 41–72.

Cassidy, N. J., and T. M. Millington, 2009, The application of finite-difference time-domain modelling for the assessment of GPR in magnetically lossy materials: Journal of Applied Geophysics, **67**, 296–308, doi: 10.1016/j.jappgeo.2008.09.009.

Ciarletti, V., C. Corbel, D. Plettemeier, P. Cais, S. M. Clifford, and S. Hamran, 2011, WISDOM GPR designed for shallow and high-resolution sounding of the Martian subsurface: Proceedings of the IEEE, **99**, 824–836, doi: 10.1109/JPROC.2010.2100790.

Coey, J. M. D., S. Morup, M. B. Madsen, and J. M. Knudsen, 1990, Titanomaghemite in magnetic soils on Earth and Mars: Journal of Geophysical Research, **95**, 14423–14425, doi: 10.1029/JB095iB09p14423.

Daniels, D. J., 2004, Ground penetrating radar: IEEE.

Di Matteo, A., E. Pettinelli, and E. Slob, 2013, Early-time GPR signal attributes to estimate soil dielectric permittivity: A theoretical study: IEEE Transactions on Geoscience and Remote Sensing, **51**, 1643–1654, doi: 10.1109/TGRS.2012.2206817.

Grant, J. A., A. E. Schutz, and B. A. Campbell, 2003, Ground-penetrating radar as a tool for probing the shallow subsurface of Mars: Journal of Geophysical Research, **108**, 8024, doi: 10.1029/2002JE001856.

Grosvenor, C. A., R. T. Johnk, J. Baker-Jarvis, M. D. Janezic, and B. Riddle, 2009, Time-domain free-field measurements of the relative permittivity of building materials: IEEE Transactions on Instrumentation and Measurement, **58**, 2275–2282, doi: 10.1109/TIM.2009.2013916.

Jackson, T. J., D. M. Le Vine, A. Y. Hsu, A. Oldak, P. J. Starks, C. T. Swift, J. D. Isham, and M. Haken, 1999, Soil moisture mapping at regional scales using microwave radiometry: The Southern Great Plains Hydrology Experiment: IEEE Transactions on Geoscience and Remote Sensing, **37**, 2136–2151, doi: 10.1109/36.789610.

Jol, H. M., C. D. Peterson, S. Vanderburgh, and J. Phipps, 1998, GPR as a regional geomorphic mapping tool: Shoreline accretion/erosion along the Columbia River littoral cell: Presented at Seventh International Conference on Ground-Penetrating Radar, 257–262.

Josh, M., M. J. Lintern, A. W. Kepic, and M. Verrall, 2011, Impact of grain-coating iron minerals on dielectric response of quartz sand and implications for ground-penetrating radar: Geophysics, **76**, no. 5, J27–J34, doi: 10.1190/geo2010-0321.1.

Keller, G. V., 1987, Rock and mineral properties, *in* M. N. Nabighian, ed., Electromagnetic methods in applied geophysics: SEG, Investigations in Geophysics 3, 13–51.

Klein, K., and J. C. Santamarina, 2000, Ferromagnetic inclusions in geomaterials: Implications: Journal of Geotechnical and Geoenvironmental Engineering, **126**, 167–179, doi: 10.1061/(ASCE)1090-0241(2000)126:2(167).

Komar, P. D., and C. Wang, 1984, Process of selective grain transport and the formation of placers on beaches: Journal of Geology, **92**, 637–655, doi: 10.1086/628903.

Kutrubes, D. L., 1986, Dielectric permittivity measurements of soils saturated with hazardous fluids: M.S. thesis, Colorado School of Mines.

Leuschen, C., P. Kanagaratnam, K. Yoshikawa, S. A. Arcone, and P. Gogineni, 2003, Design and field experiments of a ground-penetrating radar for Mars exploration: Journal of Geophysical Research, **108**, 8034, doi: 10.1029/2002JE001876.

Liu, L., and S. A. Arcone, 2003, Numerical simulation of the wave-guide effect of the near-surface thin layer on radar wave propagation: Journal of Environmental and Engineering Geophysics, **8**, 133–141, doi: 10.4133/JEEG8.2.133.

Maher, B. A., and R. Thompson, 1995, Paleorainfall reconstructions from pedogenic magnetic susceptibility variations in the Chinese loess and paleosols: Quaternary Research, **44**, 383–391, doi: 10.1006/qres.1995.1083.

Mattei, E., A. De Santis, A. Di Matteo, E. Pettinelli, and G. Vannaroni, 2005, Time domain reflectometry of glass beads/magnetite mixtures: A time and frequency domain study: Applied Physics Letters, **86**, 224102, doi: 10.1063/1.1935029.

Moran, M. S., C. D. Peters-Lidard, J. M. Watts, and S. McElroy, 2004, Estimating soil moisture at the watershed scale with satellite-based radar and land surface models: Canadian Journal of Remote Sensing, **30**, 805–826, doi: 10.5589/m04-043.

Neal, A., 2004, Ground-penetrating radar and its use in sedimentology: Principles, problems and progress: Earth-Science Reviews, **66**, 261–330, doi: 10.1016/j.earscirev.2004.01.004.

Olhoeft, G. R., 1998, Electrical, magnetic and geometric properties that determine ground penetrating radar performance: Presented at Seventh International Conference on Ground-penetrating radar, 177–182.

Olhoeft, G. R., and D. E. Capron, 1993, Laboratory measurements of the radiofrequency electrical and magnetic properties of soils from near Yuma, Arizona: U.S. Geological Survey Open-File Report, 93–701.

Olhoeft, G. R., and D. W. Strangway, 1974, Magnetic relaxation and the electromagnetic response parameter: Geophysics, **39**, 302–311, doi: 10.1190/1.1440429.

Peterson, C. D., H. M. Jol, S. Vanderburgh, J. B. Phipps, D. Percy, and G. Gelfenbaum, 2010, Dating of late Holocene beach shoreline positions by regional correlation of coseismic retreat events in the Columbia River littoral cell, USA: Marine Geology, **273**, 44–61, doi: 10.1016/j.margeo.2010.02.003.

Pettinelli, E., G. Vannaroni, A. Cereti, A. R. Pisani, F. Paolucci, D. Del Vento, D. Dolfi, S. Riccioli, and F. Bella, 2005, Laboratory investigations into the electromagnetic properties of magnetite/silica mixtures as Martian soil simulants: Journal of Geophysical Research, **110**, E04013, doi: 10.1029/2004JE002375.

Robinson, D. A., J. P. Bell, and C. H. Batchelor, 1994, Influence of iron minerals on the determination of soil water content using dielectric techniques: Journal of Hydrology, **161**, 169–180, doi: 10.1016/0022-1694(94)90127-9.

Singer, M. J., K. L. Verosub, P. Fine, and J. TenPas, 1996, A conceptual model for the enhancement of magnetic susceptibility in soils: Quaternary International, **34–36**, 243–248, doi: 10.1016/1040-6182(95)00089-5.

Stillman, D., and G. Olhoeft, 2008, Frequency and temperature dependence in electromagnetic properties of Martian analog minerals: Journal of Geophysical Research, **113**, E09005, doi: 10.1029/2007JE002977.

Strobbia, C., and G. Cassiani, 2007, Multilayer ground-penetrating radar guided waves in shallow soil layers for estimating soil water content: Geophysics, **72**, no. 4, J17–J29, doi: 10.1190/1.2716374.

Takahashi, K., H. Preetz, and J. Igel, 2011, Soil properties and performance of landmine detection by metal detector and ground-penetrating radar — Soil characterization and its verification by a field test: Journal of Applied Geophysics, **73**, 368–377, doi: 10.1016/j.jappgeo.2011.02.008.

Topp, G. C., J. L. Davis, and A. P. Annan, 1980, Electromagnetic determination of soil water content: Measurements in coaxial transmission lines: Water Resources Research, **16**, 574–582, doi: 10.1029/WR016i003p00574.

Van Dam, R. L., B. Borchers, and J. M. H. Hendrickx, 2005, Strength of landmine signatures under different soil conditions: Implications for sensor fusion: International Journal of Systems Science, **36**, 573–588, doi: 10.1080/00207720500147800.

Van Dam, R. L., J. B. J. Harrison, D. A. Hirschfeld, T. M. Meglich, Y. Li, and R. E. North, 2008, Mineralogy and magnetic properties of basaltic substrate soils: Kaho'olawe and Big Island, Hawaii: Soil Science Society of America Journal, **72**, 244–257, doi: 10.2136/sssaj2006.0281.

Van Dam, R. L., and W. Schlager, 2000, Identifying causes of ground-penetrating radar reflections using time-domain reflectometry and sedimentological analyses: Sedimentology, **47**, 435–449, doi: 10.1046/j.1365-3091.2000.00304.x.

Van Dam, R. L., W. Schlager, M. J. Dekkers, and J. A. Huisman, 2002, Iron oxides as a cause of GPR reflections: Geophysics, **67**, 536–545, doi: 10.1190/1.1468614.

van der Kruk, J., C. M. Steelman, A. L. Endres, and H. Vereecken, 2009, Dispersion inversion of electromagnetic pulse propagation within freezing and thawing soil waveguides: Geophysical Research Letters, **36**, L18503, doi: 10.1029/2009GL039581.